Attitude and Gyro Bias Estimation by SVD-Aided EKF

Abstract

This study aims to estimate both angular state and rate gyro biases for a small satellite having multiple attitude sensors. Singular value decomposition (SVD) aided Extended Kalman filter (EKF) is presented for attitude, angular rate, and gyro bias estimation. Pre-processing the measurements of sun and magnetic field sensors in SVD method precomputes Euler angles for EKF. The rotational motion parameters of the satellite and biases of rate gyro are estimated during the EKF application of the method. In comparison with traditional approaches, pre-processing before EKF makes the filter less complex by having the measurements linear and inherently adaptive. Rate gyro biases are estimated in addition to rotational motion parameters in the presented filter with a high accuracy using an inherent adaptation rule of the pre-processing step. Unscented Kalman Filter in addition to traditional and adaptive versions of EKF are tested under the same conditions for their behavior in unfavorable situations.

Keywords: small satellite, estimation, attitude determination, gyro bias, SVD, EKF.

1. Introduction

Sensor fusion techniques using the magnetometer, sun sensor, and rate gyro measurements are commonly used in order to determine the attitude and rate. For this purpose, Kalman filter extensions can be used for precise attitude parameter estimation. However, in case of any malfunction or bias type of fault, an adaptivity rule should be defined in conventional filters. Another difficulty arising in the conventional filters is the usage of the arbitrarily chosen initial values, which might cause divergence in the filter. On the other hand, single-frame attitude determination methods are depending on the vector observations at instant times [1]. They do not use satellite dynamics or any initial conditions. As the attitude and rate estimation methods considering the dynamics have a better attitude estimation accuracy, an integration of Kalman filtering is very useful in these applications. The estimation problem of the satellite's rotational motion is nonlinear in the sense of both system and measurement functions. However, in this paper, the measurements are fused using one of the single-frame methods, which makes the filter design less complex as it uses linear measurements provided from the integration stage. Therefore, the literature is reviewed in the context of the Kalman filters in two different categories nonlinear measurements based Kalman filters, and linear measurements based Kalman filters [2]. In the first approach, the observations are based on the nonlinear models. The states and measurements have a nonlinear relation. On the other hand, in the second approach, the measurements are linear with respect to the states as they are obtained from one of the single-frame methods directly with their covariance.

1.1. Background

The nonlinear measurements are used in the traditional approach of the Kalman filter for attitude and rate estimates in [3–7]. One method is to employ accelerometers, magnetometers, and gyroscopes to estimate attitude. In [8], attitude is derived from gyroscopes via a rate integration step and from the fusion of accelerometers and magnetometers via vector matching with a gyro bias estimation assist. In [9], gyros are used with vector data to estimate attitude via a kinematics-aided adaptive filter. [10] presents another gyro-aided attitude estimation. During low sampling

rates, the performance tests of [10] based on attitude estimation using inertial and magnetic measuring devices reveal that EKF is more stable than frequently employed complementing filters. The integration of the single-frame satellite attitude determination method with Kalman filters is presented in [11,12], where an EKF and algebraic method are integrated for attitude and rate estimation. The algebraic method uses 2 vectors to determine the coarse attitude [13]. The study in [14] presents a filtering scheme based on tri-axial attitude determination (TRIAD) and unscented Kalman filter (UKF) algorithms for accurate attitude satellite estimations and real-time magnetometer calibration.

The Kalman filter technique to state estimation is extremely sensitive to uncertainties and faults. If the situation of the real system does not match the models used in the filter's synthesis, then these discrepancies, which might cause sensor and actuator failures or other uncertainties in the models, drastically reduce the performance. In such instances, the KF can be modified and Adaptive or Robust Kalman Filters can be used to adjust for uncertainty and recover potential faults.

One of the challenges for attitude filters is adjusting the filter in terms of system noise covariance. Changes in the filter's system noise covariance are induced by variations in disturbance torques such as residual magnetic torque, noise on the dynamics, and actuator failures. As a result, a Robust EKF (REKF) method that scales the filter's system noise covariance can be used. Different approaches can be used to compute scaling parameters [15–17]. A variational Bayesian-based Adaptive EKF algorithm is presented in [18] for cooperative navigation of master-slave autonomous underwater vehicles. The projected error covariance and measurement noise covariance matrices, also known as Inverse Wishart priors, are generated alongside the system states using variational Bayesian approximation. Using the predicted error covariance matrix instead of process noise parameters allows the state estimate to account for both noise change and anticipated covariance changes. As a result, the proposed filter enhances the robustness against unknown or time-varying disturbances. The work [19] provides a robust adaptive UKF to improve the accuracy and robustness of state estimation when the noise covariance is uncertain. An online fault-detection technique is utilized to decide whether or not to update the current noise covariance. If necessary, the estimations of current noise covariance of process and measurement are determined using the innovation-based methodology and the residual-based method, respectively. The filter uses a weighting factor to combine the old noise covariance matrices with the estimations for the new noise covariance matrices. The authors propose a robust UKF approach for calculating pico-satellite attitude in [20]. The approach is based on a covariance matching method that modifies the UKF's measurement noise covariance matrix with a set of scale factors. The fault in the measurements is detected first with a certain statistical function, and the filter then becomes robust with the resulting scale factors. This method is also tested for an EKF, and the results are compared to the UKF.

1.2. Related Works

Vector observations and gyro measurements based Kalman filtering algorithm is presented in [21] for spacecraft attitude and gyro drift bias estimation by combining a matrix Kalman filter and cubature Kalman filter. An attitude estimation method based on a non-traditional approach, SVD/EKF is presented in [22] that uses magnetometer and sun sensor measurements onboard without any gyros considered. In that study, it is concluded that the SVD/EKF based on the linear measurements has a better accuracy performance most of the time than the traditional approach.

The approach considered in that study is not to use gyros for possible faults on the gyro measurements whereas, in this study, we estimate the biases on the gyros so as to eliminate the faults by removing them from the measurements. Therefore, the fundamental difference is in the design of the filter based on the measurements considered. But also, another approach based on a robust filter is introduced in this paper. The paper in [23] presents an SVD/UKF method where the SVD method determines the quaternions with their covariance and sends them to the UKF as linear measurements. Additionally, gyroscopes can be added to the filtering stage after processing the single-frame method. SVD method utilizes two sensors, the sun sensor, and magnetometer, which compute the attitude angles of the satellite for EKF in addition to the angular rate of the satellite from the third attitude sensor rate gyros [24]. A magnetometer calibration method aided by gyros is proposed in [25]. As the gyro measurement bias accumulates over time, the proposed method is designed so that the algorithm is robust against gyro biases by using the relative attitude information. [26] presents an estimation scheme for the attitude and the gyro bias with a series of two-dimensional measurements of the Earth's magnetic field coupled with the attitude kinematics. A Kalman-type filter based on magnetometer and gyro sensor fusion is proposed in [27] for a gyro saturation scenario in an attitude estimation problem of a spinning spacecraft. An attitude estimation algorithm that is robust against external acceleration and magnetic anomalies by online detection is proposed in [28] based on magnetic, angular rate, and gravity sensors. Another robust estimation filter is proposed in [29] by using an inertial measurement unit. It is suggested to use multiple tuning factors for each measurement axis over a single factor.

1.3. Contributions of this Study

In this study, SVD, which is one of the single-frame method, and EKF are integrated in order to estimate the satellite's attitude and rates. Besides, the biases on the rate gyros are also estimated in the augmented states. The attitude measurements by SVD are processed with their covariance in EKF for improving the attitude estimation accuracy. The most important advantage of the presented algorithm is that it gives a measurement variance updated at each step which makes the filter adaptive in addition to having linear measurements. The filtering algorithm is also tested for different cases of gyro biases. Even though UKF is superior in most cases, EKF is still in use, especially on spacecraft missions. We therefore implement a filter extension (R-adaptive EKF) that is adaptive in case of measurement faults by also conserving the base filter as EKF for a fair comparison to SVD-Aided EKF and UKF.

This paper is built upon the foundations of trying to solve several issues with the conventional filters and related works that can be listed as,

- Making the design of the filtering stage less complex by using linear measurements,
- Inherent adaptation rule integrated into the filter for malfunction or faulty cases in measurements instead of using an external adaptivity rule,
- Removing the divergence effect caused by the arbitrarily chosen initial values that might be grossly different from the correct values,
- Reconfigurable filtering design that is not affected by the sensor type or the sequence of the attitude measurements,
- Augmented state definition for the rate gyro bias estimation in integrated filters.

The aim of the paper is to estimate angular state and rate gyro bias simultaneously using an inherently adaptive filter and adaptive filter with an external rule, and to use SVD-Aided EKF with

prominent features over the traditional approach and related works presented in this paper. As Euler angles are in use for aerospace operations [30–33], the problems arose from the singularities need to be further investigated. We, therefore, utilize the Euler angles for attitude representation

The rest of the paper is organized as follows. In section 2, the satellite's rotational motion is given (kinematic and dynamic model) first. In section 3, the measurement models including sun sensor, magnetometer, and rate gyro are given. The estimation algorithm including the SVD method and EKF based on linear measurements is given in the next section, which also includes a block schema on how the measurements are fused into the SVD and used in the filtering stage. Results of the numerical simulations are discussed in section 5 and a performance evaluation of the proposed filter is presented in section 6. Conclusion remarks are presented in section 7.

2. Satellite's Rotational Motion

The attitude of the satellite can be represented using Euler angles. Then, the state vector can be composed of roll (φ), pitch (θ), yaw (ψ) angles, and angular rates on x, y, z axes,

$$\bar{\mathbf{x}} = \begin{bmatrix} \varphi & \theta & \psi & \omega_x & \omega_y & \omega_z \end{bmatrix}^T \tag{1}$$

The angular rates of body frame with respect to inertial frame,

$$\bar{\boldsymbol{\omega}}_{BI} = \begin{bmatrix} \omega_x & \omega_y & \omega_z \end{bmatrix}^T, \tag{2}$$

The rotational dynamics of the satellite can be derived by using the angular momentum conservation law;

$$J_x \frac{d\omega_x}{dt} = N_x + \left(J_y - J_z\right)\omega_y\omega_z, \tag{3a}$$

$$J_y \frac{d\omega_y}{dt} = N_y + \left(J_z - J_x\right)\omega_z\omega_x, \tag{3b}$$

$$J_z \frac{d\omega_z}{dt} = N_z + \left(J_x - J_y\right)\omega_x\omega_y, \tag{3c}$$

Here, J_x, J_y and J_z are the elements of the principal moments of inertia and N_x, N_y and N_z are external moment elements.

The satellite's kinematic equations of motion can be given using 3-2-1 Euler angle representation as,

$$\begin{bmatrix} \dot{\varphi} \\ \dot{\theta} \\ \dot{\psi} \end{bmatrix} = \begin{bmatrix} 1 & s(\varphi)t(\theta) & c(\varphi)t(\theta) \\ 0 & c(\varphi) & -s(\varphi) \\ 0 & s(\varphi)/c(\theta) & c(\varphi)/c(\theta) \end{bmatrix} \begin{bmatrix} p \\ q \\ r \end{bmatrix}. \tag{4}$$

The reason for using Euler angle representation is to particularly evaluate the singularity effect of the Euler angles. Here, $c(\cdot)$, $s(\cdot)$ and $t(\cdot)$ are the cosine, sine, and tangent functions and p, q and r are the components of $\bar{\boldsymbol{\omega}}_{BR}$ that is the angular velocity of the body frame with respect to the reference frame. $\bar{\boldsymbol{\omega}}_{BI}$ and $\bar{\boldsymbol{\omega}}_{BR}$ have a relation as,

$$\bar{\boldsymbol{\omega}}_{BR} = \bar{\boldsymbol{\omega}}_{BI} - \mathbf{A}\begin{bmatrix} 0 & -\omega_o & 0 \end{bmatrix}^T, \tag{5}$$

where $\mathbf{A}$ is the transformation matrix from orbit to body coordinate system, ω_o is the angular

velocity of the orbit.

3. Attitude and Rate Measurement Models

In this study, the sun sensor and magnetometer are used as attitude sensors whereas rate gyro measurements are used in angular rate estimation procedures.

3.1. Sun Sensor Measurement Model

The reference sun direction can be calculated in the inertial frame at a specified time [34] which can then be transformed into orbit coordinates. The sun sensor measurements can be modeled by the transformed reference sun direction from orbit to body coordinates using the attitude transformation matrix $\mathbf{A}$ as,

$$\mathbf{S}_m(k) = \mathbf{A}(k)\mathbf{S}_o(k) + \boldsymbol{\upsilon}_S(k) \tag{6}$$

where $\mathbf{S}_m$ is the sun sensor measurement vector, $\mathbf{S}_o$ is the reference sun direction vector in orbit coordinates, and $\boldsymbol{\upsilon}_S$ is the zero-mean Gaussian noise of the sun sensor measurements. The sun sensor gives zero-output during the eclipse. Therefore, $\mathbf{S}_m = 0$ in the dark side of the planet.

3.2. Magnetometer Measurement Model

As the magnetic field reference direction, International Geomagnetic Reference Field (IGRF) is used [35]. The position of the near-Earth spacecraft and the time information are necessary for calculating the reference magnetic field vector $\mathbf{B}_o$ in orbit coordinates. The magnetometer measurements can be modeled by the transformed reference magnetic field using the attitude transformation matrix $\mathbf{A}$ as,

$$\mathbf{B}_m(k) = \mathbf{A}(k)\mathbf{B}_o(k) + \boldsymbol{\upsilon}_B(k) \tag{7}$$

where $\mathbf{B}_m$ is the magnetometer measurement vector and $\boldsymbol{\upsilon}_B$ is the zero-mean Gaussian noise of the magnetometer measurements.

3.3. Rate Gyro Measurement Model

Gyroscopes are used for the angular rate measurements on each axis. They can be modeled using the following formula,

$$\bar{\boldsymbol{\omega}}_{BI,m} = \bar{\boldsymbol{\omega}}_{BI} + \bar{\mathbf{b}}_g + \boldsymbol{\eta}, \tag{8}$$

where $\bar{\boldsymbol{\omega}}_{BI,m}$ represents the body frame angular rates with respect to inertial frame, $\bar{\mathbf{b}}_g$ denotes the gyro biases as $\bar{\mathbf{b}}_g = \begin{bmatrix} b_{g_x} & b_{g_y} & b_{g_z} \end{bmatrix}^T$ and $\boldsymbol{\eta}$ is zero mean Gaussian noise with characteristics of

$$E\left[\eta_k \eta_j^T\right] = I_{3x3}\sigma_g^2 \delta_{kj}. \tag{9}$$

where $\boldsymbol{\sigma}_g$ is the standard deviation of rate gyro, δ_{ij} is the Kronecker's delta symbol. Nevertheless, characteristics of gyro bias are given as,

$$\frac{d\bar{\mathbf{b}}_g}{dt} = \boldsymbol{\eta}_2, \tag{10}$$

where $\boldsymbol{\eta}_2$ is also the zero mean Gaussian noise with characteristics of

$$E\left[\eta_{2k}\eta_{2j}^{T}\right]=I_{3x3}\sigma_{gb}^{2}\delta_{kj}. \tag{11}$$

Here, $\boldsymbol{\sigma}_{gb}$ is the standard deviation of gyro biases.

4. Satellite Attitude Estimation using EKF Based on Linear Measurements

4.1. SVD Method

The loss function defined by Wahba can be minimized using single-frame methods [36]. As it can be seen in (12), the difference between the unit vectors of the reference directions and the measurements expresses the loss,

$$L(\mathbf{A})=\frac{1}{2}\sum_{i}a_{i}\left|\mathbf{b}_{i}-\mathbf{A}\mathbf{r}_{i}\right|^{2}, \tag{12}$$

Here, a_i is the non-negative weight set, $\mathbf{b}_i$ is the unit vector of the measurements in the body frame, $\mathbf{r}_i$ is the unit vector of the models in the reference frame, $\mathbf{A}$ is the attitude transformation matrix. We can now define a matrix $\mathbf{B}$,

$$\mathbf{B}=\sum a_{i}\mathbf{b}_{i}\mathbf{r}_{i}^{T}, \tag{13}$$

By the definition of the matrix $\mathbf{B}$, the loss function can be formed as,

$$L\left(\mathbf{A}\right)=\lambda_{0}-tr\left(\mathbf{A}\mathbf{B}^{T}\right) \tag{14}$$

where $\lambda_0=\sum a_i$. In order to minimize the loss function, the SVD method is used [32,33].

$$\mathbf{B}=\mathbf{U}\mathbf{S}\mathbf{V}^{T}=\mathbf{U}\mathrm{diag}\left|S_{11}\;S_{22}\;\mathrm{S}_{33}\right|\mathbf{V}^{T}, \tag{15}$$

$$\mathbf{A}_{opt}=\mathbf{U}\mathrm{diag}[1\quad 1\quad \det(\mathbf{U})\det(\mathbf{V})]\mathbf{V}^{T}. \tag{16}$$

where $\mathbf{U}$ and $\mathbf{V}$ are orthogonal matrices. The attitude can be obtained from the optimal attitude matrix $\mathbf{A}_{opt}$. The determined attitude values can be used as the initial values in the filtering stage This usage is expected to remove the divergence effect because of the arbitrarily chosen initial conditions that might be grossly different from the correct value. Primary and secondary singular values can be defined as $(\mathrm{S}_{11},\mathrm{S}_{22},\mathrm{S}_{33})$ and $(\mathrm{s}_{11},\mathrm{s}_{22},\mathrm{s}_{33})$ respectively. The secondary singular values are calculated as $s_1=S_{11},\ s_2=S_{22},\ s_1=\det(\mathbf{U})\det(\mathbf{V})S_{33}$. The covariance matrix of determined attitude angles $(\mathbf{P}_{svd})$,

$$\mathbf{P}_{svd}=\mathbf{U}diag[(\mathrm{s}_{2}+\mathrm{s}_{3})^{-1}\quad(\mathrm{s}_{3}+\mathrm{s}_{1})^{-1}\quad(\mathrm{s}_{1}+\mathrm{s}_{2})^{-1}]\mathbf{U}^{T} \tag{17}$$

which is used as the attitude measurement error covariance matrix in the filtering stage. The details on obtaining the covariance as a statistical measure can be found in [39].

In this study, magnetic field and sun directions are used as the reference directions. IGRF is used for the geomagnetic field model [35] with the inputs of the spacecraft's position and time. The orbit is propagated using the model presented in [40]. The magnetic field vector is normalized afterward. Using the same inputs sun direction can be obtained as a unit vector [34]. Using these two reference directions and the measurements, the satellite's attitude angles can be determined.

4.2. EKF Design for Linear Measurements

When designing EKF based on linear measurements, attitude angle measurements that characterize the satellite's attitude, are determined using the SVD method [24],

$$z_{\varphi_i}=\varphi_i+\mathrm{v}_{\varphi_i},\ z_{\theta_i}=\theta_i+\mathrm{v}_{\theta_i},\ z_{\psi_i}=\psi_i+\mathrm{v}_{\psi_i}, \tag{18}$$

where $\mathrm{v}_{(\cdot)_i}$ is the attitude measurement noise of SVD. The mathematical expectations and variances are $E[\mathrm{v}]=0$, $E\left[\mathrm{v}_{\varphi_i},\mathrm{v}_{\varphi_j}\right]=D_{\varphi_i}\delta_{ij}$, $E\left[\mathrm{v}_{\theta_i},\mathrm{v}_{\theta_j}\right]=D_{\theta_i}\delta_{ij}$ and $E\left[\mathrm{v}_{\psi_i},\mathrm{v}_{\psi_j}\right]=D_{\psi_i}\delta_{ij}$.
The equation (18) reflects the determined attitude by the SVD method, which is used as attitude measurements in the filter. The measurement error covariance $\mathbf{R}$ is also obtained from the SVD method and updated every time step. The measurement error covariance is not an arbitrarily chosen value but follows Wahba's problem-based SVD method rule defined in (17). Here, it should be noted that the roll-pitch-yaw correlates in reality; however, as the Kalman filter uses diagonal covariance matrix inherently, a sub-decomposition stage e.g. UD-decomposition is necessary to compose a new measurement matrix and corresponding covariance [41]. In the paper, this stage is assumed to be negligible.

The angular velocities $\omega_x,\omega_y,\omega_z$ of the satellite are measured using the rate gyroscopes. The augmented output vector can be built as,

$$\bar{\mathbf{U}}=\left[\varphi \quad \theta \quad \psi \quad \omega_x \quad \omega_y \quad \omega_z \quad b_{g_x} \quad b_{g_y} \quad b_{g_z}\right]^T, \tag{19}$$

then, the mathematical model can be linearized as,

$$\mathbf{U}_i = f\left(\hat{\mathbf{U}}_{i-1},\bar{\omega}_{o_{i-1}}\right)+\mathbf{F}_{U_{i-1}}\left(\mathbf{U}_{i-1}-\hat{\mathbf{U}}_{i-1}\right)+\mathbf{F}_o\left(\bar{\omega}_{o_{i-1}}-\omega_{o_{i-1}}^{comp}\right), \tag{20}$$

where θ_i, ψ_i, φ_i - are pitch, yaw, and roll angles respectively; ω_{x_i}, ω_{y_i}, ω_{z_i} - are angular rates; $f\left(\hat{\mathbf{U}}_{i-1},\bar{\omega}_{o_{i-1}}\right)=\left[f_\varphi \quad f_\theta \quad f_\psi \quad f_{\omega_x} \quad f_{\omega_y} \quad f_{\omega_z} \quad f_{b_{g_x}} \quad f_{b_{g_y}} \quad f_{b_{g_z}}\right]^T$ is the mathematical model of the spacecraft's rotational motion based on estimations, $\bar{\omega}_{o_{i-1}}$ is the orbital velocity, $\omega_{o_{i-1}}^{comp}$ is the computational value of the orbital velocity; $\mathbf{F}_o$ is system input's coefficient matrix,

$$\mathbf{F}_U = \left[\frac{\partial f}{\partial \mathbf{U}}\right]_{\hat{U}_{i-1},\bar{\omega}_{o_{i-1}}} = \begin{bmatrix}
\frac{\partial f_\varphi}{\partial \varphi} & \frac{\partial f_\varphi}{\partial \theta} & \frac{\partial f_\varphi}{\partial \psi} & \frac{\partial f_\varphi}{\partial \omega_x} & \frac{\partial f_\varphi}{\partial \omega_y} & \frac{\partial f_\varphi}{\partial \omega_z} & \frac{\partial f_\varphi}{\partial b_{g_x}} & \frac{\partial f_\varphi}{\partial b_{g_y}} & \frac{\partial f_\varphi}{\partial b_{g_z}} \\
\frac{\partial f_\theta}{\partial \varphi} & \frac{\partial f_\theta}{\partial \theta} & \frac{\partial f_\theta}{\partial \psi} & \frac{\partial f_\theta}{\partial \omega_x} & \frac{\partial f_\theta}{\partial \omega_y} & \frac{\partial f_\theta}{\partial \omega_z} & \frac{\partial f_\theta}{\partial b_{g_x}} & \frac{\partial f_\theta}{\partial b_{g_y}} & \frac{\partial f_\theta}{\partial b_{g_z}} \\
\frac{\partial f_\psi}{\partial \varphi} & \frac{\partial f_\psi}{\partial \theta} & \frac{\partial f_\psi}{\partial \psi} & \frac{\partial f_\psi}{\partial \omega_x} & \frac{\partial f_\psi}{\partial \omega_y} & \frac{\partial f_\psi}{\partial \omega_z} & \frac{\partial f_\psi}{\partial b_{g_x}} & \frac{\partial f_\psi}{\partial b_{g_y}} & \frac{\partial f_\psi}{\partial b_{g_z}} \\
\frac{\partial f_{\omega_x}}{\partial \varphi} & \frac{\partial f_{\omega_x}}{\partial \theta} & \frac{\partial f_{\omega_x}}{\partial \psi} & \frac{\partial f_{\omega_x}}{\partial \omega_x} & \frac{\partial f_{\omega_x}}{\partial \omega_y} & \frac{\partial f_{\omega_x}}{\partial \omega_z} & \frac{\partial f_{\omega_x}}{\partial b_{g_x}} & \frac{\partial f_{\omega_x}}{\partial b_{g_y}} & \frac{\partial f_{\omega_x}}{\partial b_{g_z}} \\
\frac{\partial f_{\omega_y}}{\partial \varphi} & \frac{\partial f_{\omega_y}}{\partial \theta} & \frac{\partial f_{\omega_y}}{\partial \psi} & \frac{\partial f_{\omega_y}}{\partial \omega_x} & \frac{\partial f_{\omega_y}}{\partial \omega_y} & \frac{\partial f_{\omega_y}}{\partial \omega_z} & \frac{\partial f_{\omega_y}}{\partial b_{g_x}} & \frac{\partial f_{\omega_y}}{\partial b_{g_y}} & \frac{\partial f_{\omega_y}}{\partial b_{g_z}} \\
\frac{\partial f_{\omega_z}}{\partial \varphi} & \frac{\partial f_{\omega_z}}{\partial \theta} & \frac{\partial f_{\omega_z}}{\partial \psi} & \frac{\partial f_{\omega_z}}{\partial \omega_x} & \frac{\partial f_{\omega_z}}{\partial \omega_y} & \frac{\partial f_{\omega_z}}{\partial \omega_z} & \frac{\partial f_{\omega_z}}{\partial b_{g_x}} & \frac{\partial f_{\omega_z}}{\partial b_{g_y}} & \frac{\partial f_{\omega_z}}{\partial b_{g_z}} \\
\frac{\partial f_{b_{g_x}}}{\partial \varphi} & \frac{\partial f_{b_{g_x}}}{\partial \theta} & \frac{\partial f_{b_{g_x}}}{\partial \psi} & \frac{\partial f_{b_{g_x}}}{\partial \omega_x} & \frac{\partial f_{b_{g_x}}}{\partial \omega_y} & \frac{\partial f_{b_{g_x}}}{\partial \omega_z} & \frac{\partial f_{b_{g_x}}}{\partial b_{g_x}} & \frac{\partial f_{b_{g_x}}}{\partial b_{g_y}} & \frac{\partial f_{b_{g_x}}}{\partial b_{g_z}} \\
\frac{\partial f_{b_{g_y}}}{\partial \varphi} & \frac{\partial f_{b_{g_y}}}{\partial \theta} & \frac{\partial f_{b_{g_y}}}{\partial \psi} & \frac{\partial f_{b_{g_y}}}{\partial \omega_x} & \frac{\partial f_{b_{g_y}}}{\partial \omega_y} & \frac{\partial f_{b_{g_y}}}{\partial \omega_z} & \frac{\partial f_{b_{g_y}}}{\partial b_{g_x}} & \frac{\partial f_{b_{g_y}}}{\partial b_{g_y}} & \frac{\partial f_{b_{g_y}}}{\partial b_{g_z}} \\
\frac{\partial f_{b_{g_z}}}{\partial \varphi} & \frac{\partial f_{b_{g_z}}}{\partial \theta} & \frac{\partial f_{b_{g_z}}}{\partial \psi} & \frac{\partial f_{b_{g_z}}}{\partial \omega_x} & \frac{\partial f_{b_{g_z}}}{\partial \omega_y} & \frac{\partial f_{b_{g_z}}}{\partial \omega_z} & \frac{\partial f_{b_{g_z}}}{\partial b_{g_x}} & \frac{\partial f_{b_{g_z}}}{\partial b_{g_y}} & \frac{\partial f_{b_{g_z}}}{\partial b_{g_z}}
\end{bmatrix}$$

$$\mathbf{F}_o = \left[\frac{\partial f}{\partial \omega_o}\right]_{\hat{U}_{i-1},\bar{\omega}_{o_{i-1}}} = \begin{bmatrix} 0 & -\Delta t & 0 & 0 & 0 & 0 & 0 & 0 & 0 \end{bmatrix}^T \tag{21}$$

Here Δt is the sample time.

The optimum criterion can be selected from the minimum standard deviation, and the satellite's attitude estimation algorithm can be shaped using Bayes' method. The conditional probability density function of $p\left(\mathbf{U}_i/\overline{\mathbf{z}}_i,\bar{\omega}_{o_i}\right)$ should be evaluated and can be written to the Bayes formula as [[24],

$$p\left(\mathbf{U}_i/\mathbf{Z}^i,\bar{\omega}_{o_i}\right) = p\left(\mathbf{U}_i/\mathbf{Z}^{i-1},\mathbf{z}_i,\bar{\omega}_{o_i}\right) = \frac{p\left(\mathbf{U}_i/\mathbf{Z}^{i-1},\bar{\omega}_{o_i}\right)p\left(\mathbf{z}_i/\mathbf{U}_i,\mathbf{Z}^{i-1},\bar{\omega}_{o_i}\right)}{p\left(\mathbf{z}_i/\mathbf{Z}^{i-1}\right)}, \tag{22}$$

where $\mathbf{z}_i^T = \left[z_{\varphi_i}, z_{\theta_i}, z_{\psi_i}, z_{\omega_{xi}}, z_{\omega_{yi}}, z_{\omega_{zi}}\right]$ is the measurement vector; $\mathbf{Z}^i = \{\mathbf{z}_1 \quad \mathbf{z}_2 \quad \ldots \quad \mathbf{z}_i\}$, $\mathbf{Z}^{i-1} = \{\mathbf{z}_1 \quad \mathbf{z}_2 \quad \ldots \quad \mathbf{z}_{i-1}\}$.

By taking the minimum standard deviation as the optimum criterion, and $p\left(\mathbf{U}_i/\mathbf{Z}^i,\bar{\omega}_{o_i}\right)$, as a Gauss distribution into account, the recursive scheme for attitude estimation is found as,

$$\hat{\mathbf{U}}_i = f\left(\hat{\mathbf{U}}_{i-1},\bar{\omega}_{o_{i-1}}\right) + \mathbf{K}_i\left[\mathbf{z}_i - \mathbf{H}f\left(\hat{\mathbf{U}}_{i-1},\bar{\omega}_{o_{i-1}}\right)\right], \tag{23}$$

$$\mathbf{\Delta}_i = \mathbf{z}_i - \mathbf{H}f\left(\hat{\mathbf{U}}_{i-1},\bar{\omega}_{o_{i-1}}\right), \tag{24}$$

$$\mathbf{P}_i^{+} = \left[\mathbf{I} - \mathbf{K}_i\mathbf{H}\right]\mathbf{P}_i^{-1}, \tag{25}$$

$$\mathbf{K}_i = \mathbf{P}_i^{-}\mathbf{H}^T\left[\mathbf{H}\mathbf{P}_i^{-}\mathbf{H}^T + \mathbf{R}_i\right]^{-1}, \tag{26}$$

$$\mathbf{P}_i^{-} = \mathbf{F}_U\mathbf{P}_{i-1}^{+}\mathbf{F}_U^T + \mathbf{F}_o\mathbf{D}_{o_{i-1}}\mathbf{F}_o^T + \mathbf{G}\mathbf{Q}\mathbf{G}^T, \tag{27}$$

where $\mathbf{P}_i^{-}$ is the prediction error covariance matrix, $\mathbf{P}_i^{+}$ is the estimation error covariance matrix, $\mathbf{K}_i$ is the Kalman gain matrix, $\mathbf{D}_{o_{i-1}}$ is uncertainty variance for the calculated orbital velocity of the satellite, Δ_i is the innovation sequence, $\mathbf{R}_i$ is the measurement noise covariance matrix, $\mathbf{Q}$ is the system noise covariance matrix, $\mathbf{G}$ is the system noise transition matrix and $\mathbf{I}$ is the identity matrix. The EKF design can be seen from the equations (23) to (27) for the recursive estimation.

The structural design of the SVD-aided EKF is given in Fig. 1. The attitude measurement vectors and the vectors based on theoretical models are processed under the SVD method in the SVD-aided EKF algorithm, whereas they are directly used in the traditional EKF without any additional process. As the measurements are processed in SVD, it also provides measurement error covariance directly to the SVD-aided EKF, while traditional EKF does not have any adaptation procedure inherently.

The observability analysis of the states can be applied based on Popov–Bevelic–Hautus (PBH) criterion [42]. According to this criterion, the system defined by the system matrix as $\mathbf{F}_U$ and measurement matrix as $\mathbf{H}$ is considered state observable if and only if,

$$\mathbf{O} = \begin{bmatrix} \lambda_i\mathbf{I} - \mathbf{F}_U \\ \mathbf{H} \end{bmatrix} \tag{28}$$

has the full rank for each eigenvalue λ of the matrix $\mathbf{F}_U$ [42,43].

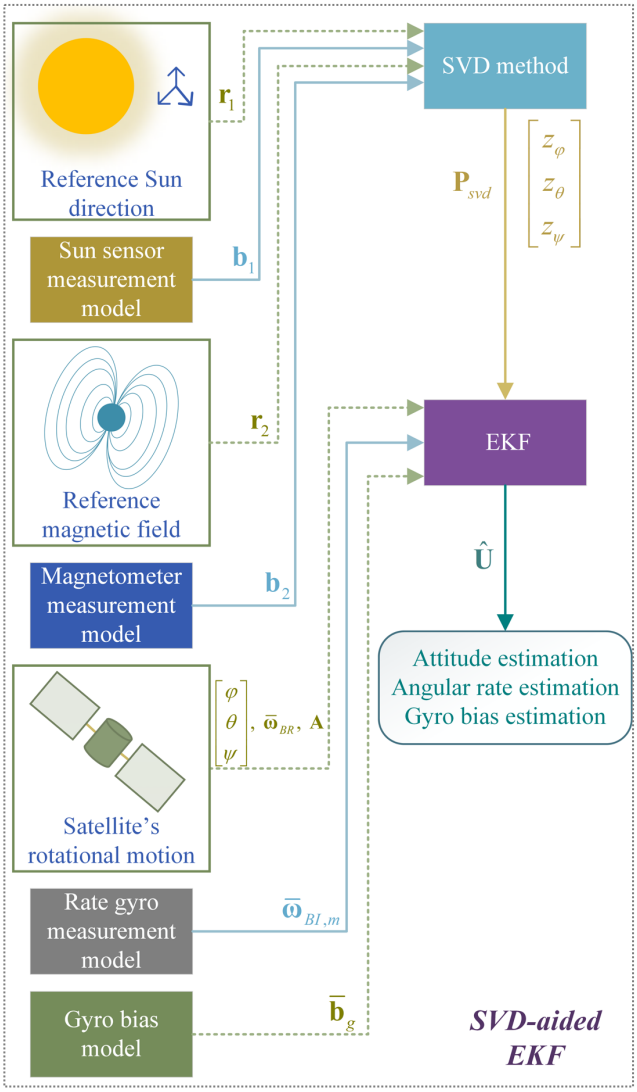

Fig. 1. Sun sensor, magnetometer, and rate gyro measurements based SVD-aided EKF algorithm's block schema.

The degree of observability (DoO) can also be defined for examining better observability [44,45]. The normalization of the error covariance matrix $\mathbf{P}_i^+$ can be performed as follows,

$$\mathbf{P}_i' = \left(\sqrt{\mathbf{P}_0}\right)^{-1} \mathbf{P}_i^+ \left(\sqrt{\mathbf{P}_0}\right)^{-1} \tag{29a}$$

where $\mathbf{P}_0$ is the initial error covariance matrix, $\mathbf{P}_i^+$ is the estimation error covariance matrix, and $\mathbf{P}_i'$ is the normalized error covariance matrix. The matrix can be rewritten to show element-by-element form as,

$$\mathbf{P}_i' = \begin{bmatrix} \dfrac{\mathbf{P}^+_{i_{11}}}{\mathbf{P}_{0_{11}}} & \dfrac{\mathbf{P}^+_{i_{12}}}{\sqrt{\mathbf{P}_{0_{11}}\mathbf{P}_{0_{22}}}} & \cdots & \dfrac{\mathbf{P}^+_{i_{1n}}}{\sqrt{\mathbf{P}_{0_{11}}\mathbf{P}_{0_{nn}}}} \\ \dfrac{\mathbf{P}^+_{i_{21}}}{\sqrt{\mathbf{P}_{0_{22}}\mathbf{P}_{0_{11}}}} & \dfrac{\mathbf{P}^+_{i_{11}}}{\mathbf{P}_{0_{22}}} & \cdots & \dfrac{\mathbf{P}^+_{i_{2n}}}{\sqrt{\mathbf{P}_{0_{22}}\mathbf{P}_{0_{nn}}}} \\ \vdots & \vdots & \ddots & \vdots \\ \dfrac{\mathbf{P}^+_{i_{n1}}}{\sqrt{\mathbf{P}_{0_{nn}}\mathbf{P}_{0_{11}}}} & \dfrac{\mathbf{P}^+_{i_{n2}}}{\sqrt{\mathbf{P}_{0_{nn}}\mathbf{P}_{0_{22}}}} & \cdots & \dfrac{\mathbf{P}^+_{i_{nn}}}{\mathbf{P}_{0_{nn}}} \end{bmatrix} \tag{29b}$$

where $\mathbf{P}^+_{i_{kl}}$ is the element of the k[th] row and l[th] column of the error covariance matrix whereas $\mathbf{P}_{0_{kl}}$ represents the initial error covariance matrix elements. The sum of all of the eigenvalues of a matrix equals to the trace of the matrix, the normalized error covariance matrix therefore is,

$$\mathbf{P}_i'' = \frac{n}{tr\left(\mathbf{P}_i'\right)}\mathbf{P}_i' \tag{30}$$

The eigenvalues of $\mathbf{P}''$ are bounded between $0 < \lambda_i \leq n$, such that the DoO is getting smaller with the decreasing error.

5. SVD-Aided Robust EKF

The essence of the measurement error adaptation technique is to compare the real and theoretical values of the innovation covariance matrix. When a sensor fails in the system, the real error exceeds the theoretical error. In this situation, we may assure the filter's robustness against sensor failure by modifying the R matrix, which is a diagonal matrix composed of measurement noise covariances. The adaptation technique essentially seeks an appropriate multiplier matrix for R such that the real and theoretical values of the innovation covariance coincide. By matching these two values, we essentially raise the R matrix's required term(s) (the term(s) corresponding to the sensor(s) with the incorrect measurement). We can incorporate a matrix composed of different scale factors, $S(k)$, into the algorithm to modify the measurement noise covariance matrix and match the real and theoretical innovation covariances,

$$\frac{1}{\xi}\sum_{j=i-\xi+1}^{i} \boldsymbol{e}_j\boldsymbol{e}_j^T = HP_i^-H^T + S_iR_i. \tag{31}$$

The scale matrix is then defined as follows,

$$S_i = \left\{\frac{1}{\xi}\sum_{j=i-\xi+1}^{i} \boldsymbol{e}_j\boldsymbol{e}_j^T - HP_i^-H^T\right\}R_i^{-1}. \tag{32}$$

Aside from the fact that the measurement noise covariance matrix must be positive definite (which is why the multiplier matrix cannot have negative terms), any term of this matrix cannot decrease in time for this specific problem because there is no way to improve the performance of the onboard sensor (that is why the multiplier S_i matrix cannot have terms less than one). To prevent such scenarios, the following rule [12] is recommended for composing the scale matrix,

$$S^* = diag\left(s_1^*, s_2^*, \ldots, s_k^*\right) \tag{33}$$

$$s_l^* = \max\left\{1, S_{ll}\right\} \qquad l = \overline{1,k}. \tag{34}$$

Here, S_{ll} represents the i[th] diagonal element of the matrix S_i.

The scale matrix is then corrected and diagonalized using Equations (32, 33). Finally, the Kalman gain is adjusted as follows,

$$K_i = P_i^- H^T \left[H P_i^- H^T + S_i^* R_i \right]^{-1} \tag{35}$$

In the event of a malfunction, the element(s) of the scale matrix corresponding to the faulty component(s) of the innovation vector rise, causing the terms in the relevant column(s) of the Kalman gain to drop. As a result, the impact of the faulty innovation channel on the state update process is reduced, and reliable estimation results can be produced even when measurement malfunctions occur.

6. Simulation Results

For the analysis, simulations were run with 1-Hz frequency or $T_s = 1\text{sec}$. A nanosatellite structure is used for the simulations at the altitude of $r = 550km$. The principal moments of inertia matrix are $J = \text{diag}\left[2.1\times10^{-3} \quad 2.0\times10^{-3} \quad 1.9\times10^{-3} \right] \text{kg m}^2$. Sun sensors and magnetometers have 1-Hz frequency too. The standard deviation for magnetometers is $\sigma_B = 0.008$ and $\sigma_S = 0.002$ for sun sensors. The time interval from 2000 to 4000 s corresponds to the eclipse; therefore, the sun sensor has zero-output in this period. Since the gyroscope selected in this study is for implementation on a nanosatellite, high accuracy is not considered required. Therefore, a gyro with 0.005 deg/s standard deviation is utilized. The true attitude angles are given in Fig. 2.

Figures from 3 to 5 give the SVD-aided EKF simulation results. Attitude angle errors for SVD and SVD-aided EKF used together are presented in Fig. 3. The errors presented in the figures are the absolute errors calculated by extracting the actual (correct) values from the estimations. The actual values are computed using the kinematic and dynamic model of the satellite's rotational motion introduced in Section II. As seen from the figure, the results from the SVD-aided EKF attitude estimation method improve the SVD's outputs. Traditional EKF copes with the eclipse period better than the SVD-Aided EKF at the beginning. Therefore, it can be said that traditional filter can be selected especially for short time eclipse periods. However, the filter fails with ongoing eclipse case. Even after the eclipse ends, it converges slower than SVD-Aided EKF. The measurements and all the other parameters are used as the same for both filters for a fair comparison. However, magnetometer-based traditional EKF can be designed so as not to be affected by the eclipse and a switching algorithm could be implemented for the zero-output failure. The traditional EKF refers to the conventional EKF applied to the estimation problem of satellite's rotational motion. In other words, it uses nonlinear measurements (there is no single-frame method stage) without any inherent adaptation or an initial value provider. The only difference in the design is to add a preprocess into the algorithm seen in Fig. 1, which provides several advantages.

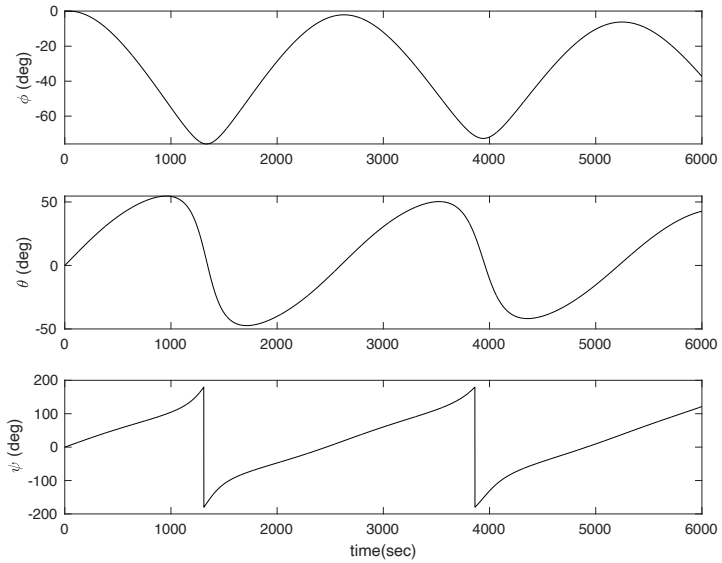

Fig. 2. True attitude angles.

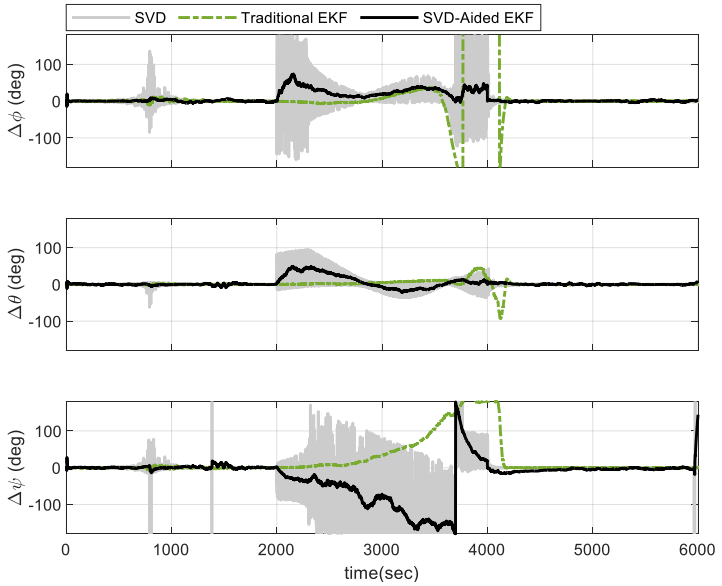

Fig. 3. Absolute errors of attitude angles.

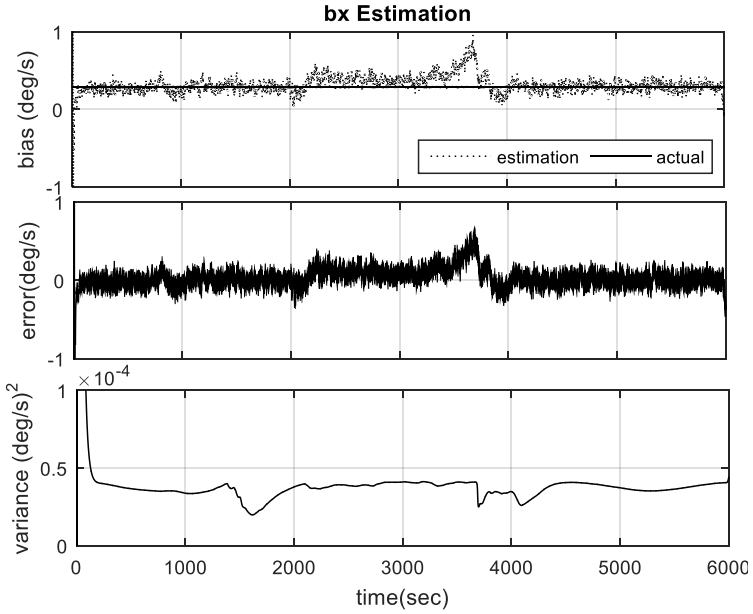

Fig. 4. Rate gyro bias estimation results on the x-axis.

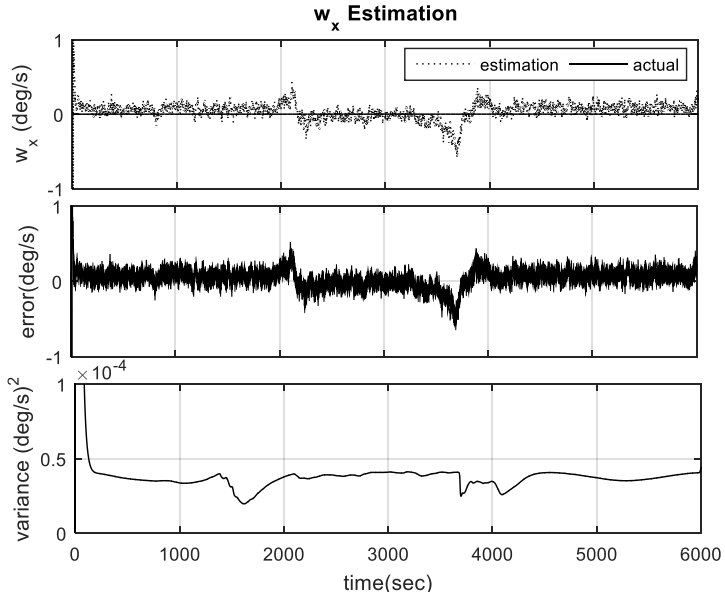

Fig. 5. Angular rate estimation results on the x-axis.

In Fig. 4, there are three panels as the estimated values of bias on the x-axis, the bias estimation errors, and variances in $\deg^2/s^2$ in x-axis. In the first panel of these figures, dots indicate the bias estimation while the black solid line gives the actual bias. It can be stated that the gyro bias is estimated accurately by looking at the behavior of approaching zero. In the third panel, variance values also support this output. The results from the y and z axes are similar and not given here for brevity.

Fig. 5 characterizes the angular rate estimation results on the x-axis. In the first panel of these figures, dots give the angular rate estimation while the black solid line indicate the actual angular rate. The estimated and actual values of the angular velocities about the x-axis, the differences between them, and the estimation error variances are shown in the second and third panels of the

figure. In the illuminated portion of the orbit, angular velocity estimation results are accurately estimated. During the eclipse period, the estimations are not completely deteriorated as in the case of the SVD method results. The results from the y and z axes are similar and not given here for brevity.

7. Discussion of the Proposed Algorithm's Properties

The properties of the proposed SVD-aided EKF attitude estimation algorithm are discussed in this section. Before moving on the discussion, the employed methods to evaluate the properties are introduced first.

Methods for the Evaluation: Some of the most encountered problems in satellite attitude estimation are evaluated in this section. One of them is the measurement faults, which might be seen in the form of zero-output failure (eclipse intervals), noise increment type of faults, etc. On the other hand, even if there is no physical fault or disturbance in the measurements, vector observations might be parallel, in which case the system acts as if there is a fault in the observations. For this reason, the times where the observations are parallel are examined. Another source of error in the case of using Euler angles might be the pitch angle approaching 90 degrees. For evaluating the filters, scenarios based on such erroneous sources are considered for analysis. The effects are handled by different types of adaptations.

The prominent features of the presented algorithm are highlighted and analyzed.

Linearity of the Measurements: In the proposed approach, EKF is designed for linear measurement equations. Hence, the filter turned into an easier structure. Also, this increases the estimation accuracy because the errors from the linearization step do not apply here.

Reconfigurability of the Measurements: The proposed algorithm needs multiple measurements but has the ability to use different measurement configurations in any step, as they are processed by the SVD first. On the other hand, the conventional EKF has to be re-designed for each configuration. The process in the SVD provides the initial conditions to the algorithm directly so it is expected to have a better convergence in the transient region than the traditional version with arbitrarily chosen initial conditions.

Robustness Against Measurement Faults: The most important advantage of the SVD-aided EKF algorithm in addition to having linear measurements is that it provides a measurement variance updated at each estimation step which makes the filter adaptive.

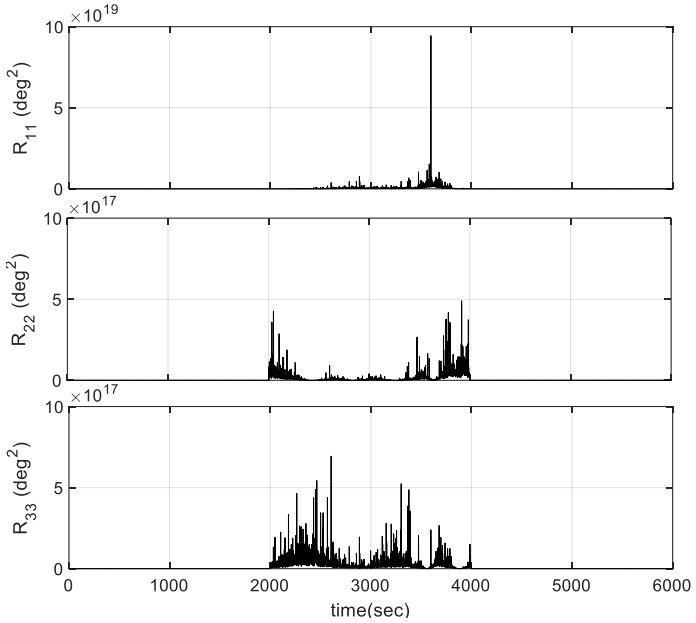

Fig. 6. Diagonal elements of the SVD-aided EKF measurement noise covariance matrix in case of zero output sensor fault.

If any fault occurs on the measurement system, the diagonal elements of the covariance matrix of measurement noise R_i that are corresponding to the attitude observations will increase. This corresponds to the filter's adaptation process. Consequently, the filter gain matrix K_i in (26) decreases, which will cause a correction in the innovation sequence of the estimation algorithm and make the estimation value of the augmented vector $\hat{U}_i$ to approach to the actual values U_i. This will lead to a decrease in innovation sequence Δ_i in (24), etc. Therefore, an adaptive scheme is performed to adjust the measurement noise covariance matrix in response to changing sensor noises. As a result, in the proposed SVD-aided EKF, satellite attitude and rate gyro bias estimation algorithm, and the changes in the measurement noise covariance are corrected by the system, without affecting the performance of estimation. Figs. 6 and 7 approve this property. The behavior of the diagonal elements of the SVD-aided EKF measurement noise covariance matrix is shown in Fig. 6. As seen, in the eclipse period (time interval from 2000 to 4000 s corresponds to the eclipse), the output of the Sun sensor is zero (zero output sensor fault occurs). Therefore, the diagonal elements of the matrix R_i increase significantly. As a result, the filter gain matrix K_i decreases, which will strengthen the corrective influence on the estimation procedure.

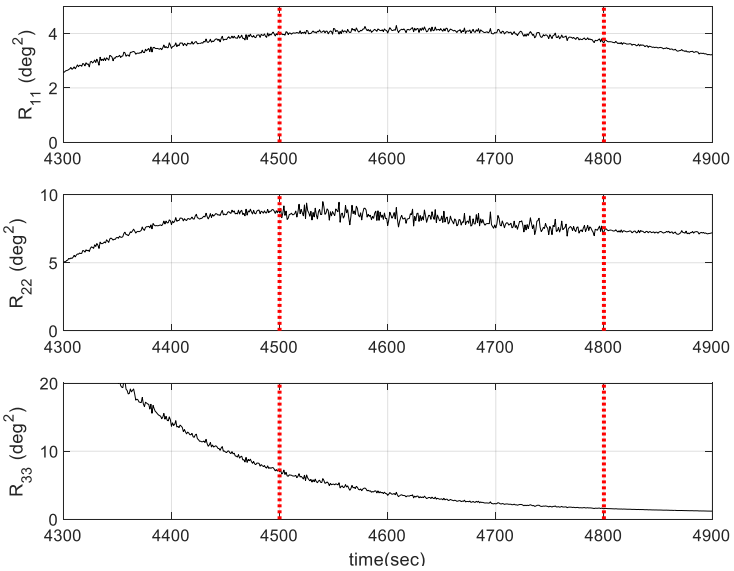

Fig. 7. Diagonal elements of the SVD-aided EKF measurement noise covariance matrix in case of noise increment sensor faults.

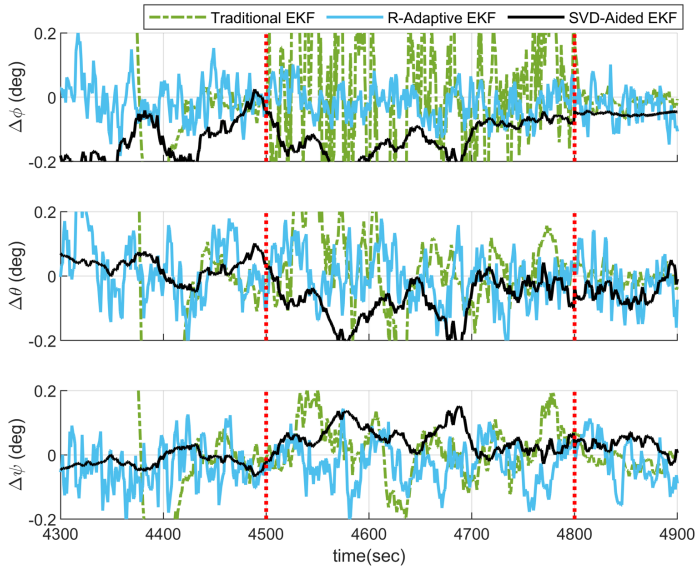

Fig. 8. Estimation error of the attitude angles in case of noise increment sensor faults.

For the next scenario, noise increment on the magnetometer measurements is applied. Magnetometer measurement noises for the x-axis are increased 10 times between 4500-4800 sec. The diagonal elements of the SVD-aided EKF measurement noise covariance matrix for this case are presented in Fig. 7. The plots show that when the noise increment fault occurs on the measurement system, the oscillatory range of the diagonal elements of the covariance matrix of measurement noise R_i increases in this specific time interval. These changes correspond to the adaptation of the filter. Another adaptive filter that adapts its R-matrix using the innovation sequence of the filter [46–48] is applied to traditional EKF for fair comparison in this scenario, and it is called R-Adaptive EKF. As a result, the estimation errors of the attitude angles by SVD-aided EKF are not affected significantly by the sensor fault and the algorithm continues to give

sufficiently good estimations whereas the traditional EKF copes with the fault with less accuracy (see Fig. 8). R-Adaptive EKF gives better results than the traditional EKF as expected and similar order of errors to the SVD-Aided EKF. The RMS errors for each method are presented in Table 1. UKF is also tested under the same conditions for presenting another Kalman-type filter yet behaving better in adverse situations than EKF, and presented in Table 1. Here, it should be kept in mind that in some cases, EKF is more computationally efficient and more stable than UKF especially for applications [49]. The noise increment period is called Period A between 4500-4800 sec. For the observability analysis, the PBH criterion is executed for the system based on Equation (28). The matrix $\mathbf{O}$ is obtained for checking if the full column rank rule is satisfied. The rank for each eigenvalue of the system matrix is found nine for each sample and even during the eclipse and the measurement fault occurrence; therefore, it can be stated that the system is state observable.

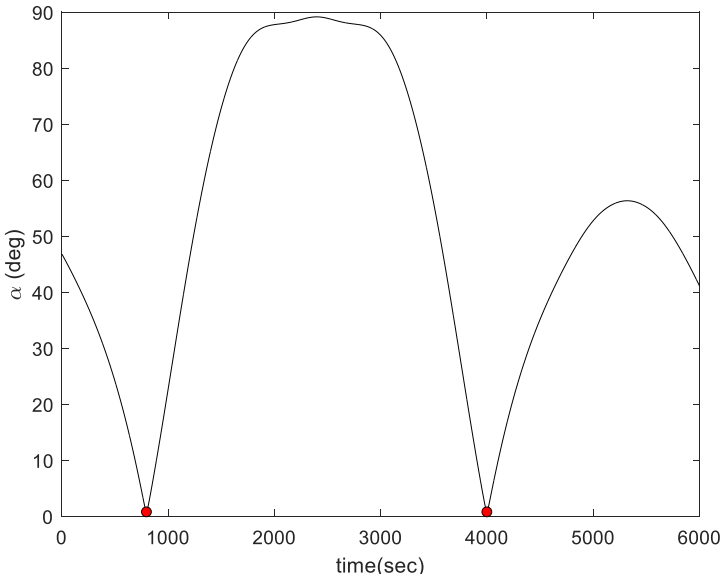

Fig. 9. The angle between two vector observations.

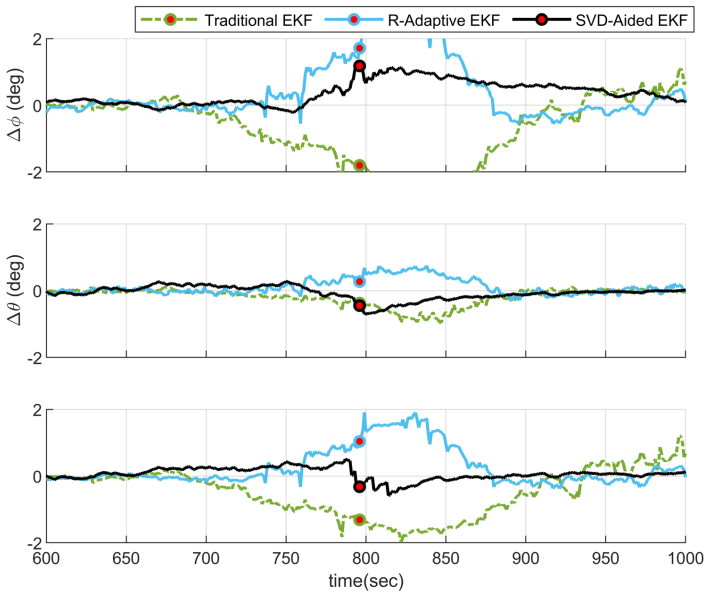

Fig. 10. Estimation error of the attitude angles in case of parallel vector observations.

Under the measurement faults, parallel vector observations are also investigated. When the angle between the vector observations is close to zero, the estimations are expected to deteriorate for some time. The angle between two measurement vectors is seen in Fig. 9. The vectors are almost parallel at 796th and 3999th seconds, which are marked with red-filled circles in the figure. As the second parallelism occurs during the eclipse close to the end, the attitude estimation errors of traditional and nontraditional EKF are demonstrated for the first parallel case in Fig. 10. The interval is seen from 600 to 1000 seconds. The estimations deteriorate more when getting closer to the marked point, where the vector observations are parallel to each other, but SVD-Aided EKF copes with the parallelism fairly well than the traditional EKF. The estimation accuracy of the filters sometimes gets very close due to randomized inputs. Therefore, the 5-simulation averaged RMS errors are calculated for Period B1:650-950 s and Period B2:3850-4150 s intervals as well (see Table I).

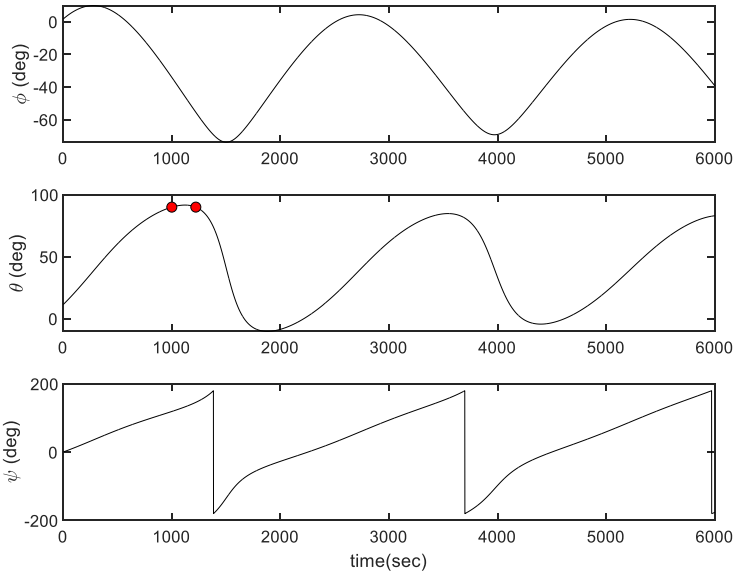

Fig. 11. The true attitude angles in the case of the pitch angle having 90^{o} values.

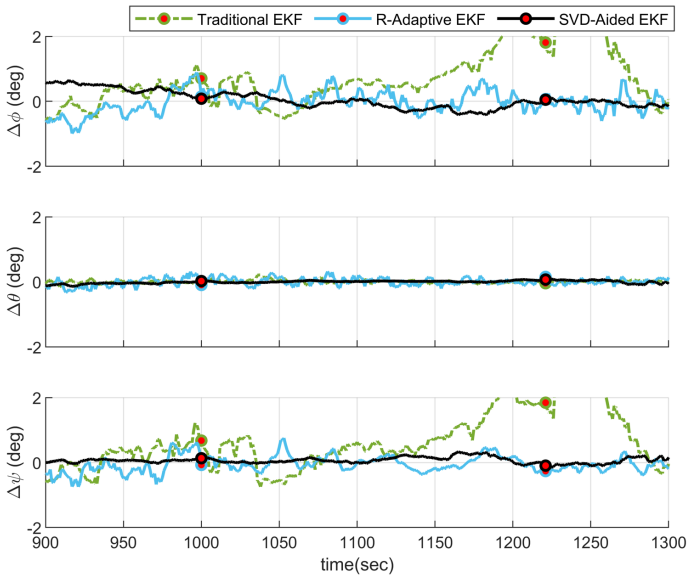

Fig. 12. Estimation error of the attitude angles in case of the pitch angle having 90º values.

Table 1. RMS errors of the attitude estimations for different periods* (averaged over 5 simulations).

RMS Errors (deg)	Period A	Period B1	Period B2	Period C1	Period C2
Traditional EKF	0.6986	0.5539	0.8429	0.2000	0.6412
UKF	0.3242	0.4838	0.8400	0.0745	0.0684
R-Adaptive EKF	0.3215	0.5466	0.8381	0.1272	0.1173
SVD-Aided EKF	0.3230	0.4963	0.8334	0.0590	0.0532

* A: Noise increment case (Period A: 4500-4800 s), B: Parallel vectors case (Period B1: 650-950 s, Period B2: 3850-4150 s), C: 90º pitch angle case (Period C1: 1000-1030 s, Period C2: 1210-1240 s).

For modeling, another error source, the case of having 90-degree values in pitch angle (singularity case in Euler angle representation) is considered by using a second set of initial conditions. The actual attitude angle for this case is seen in Fig. 11. The pitch angle is 90º at 1000th and 1221st seconds, which are marked with red-filled circles in the figure as well. The estimation errors are seen in Fig. 12 consisting of both points where the pitch angle is 90º. The superiority of the SVD-Aided EKF is very clear in this case. The associated RMS errors are presented in Table 1 as Period C1: 1000-1030 s and Period C2: 1210-1240 s.

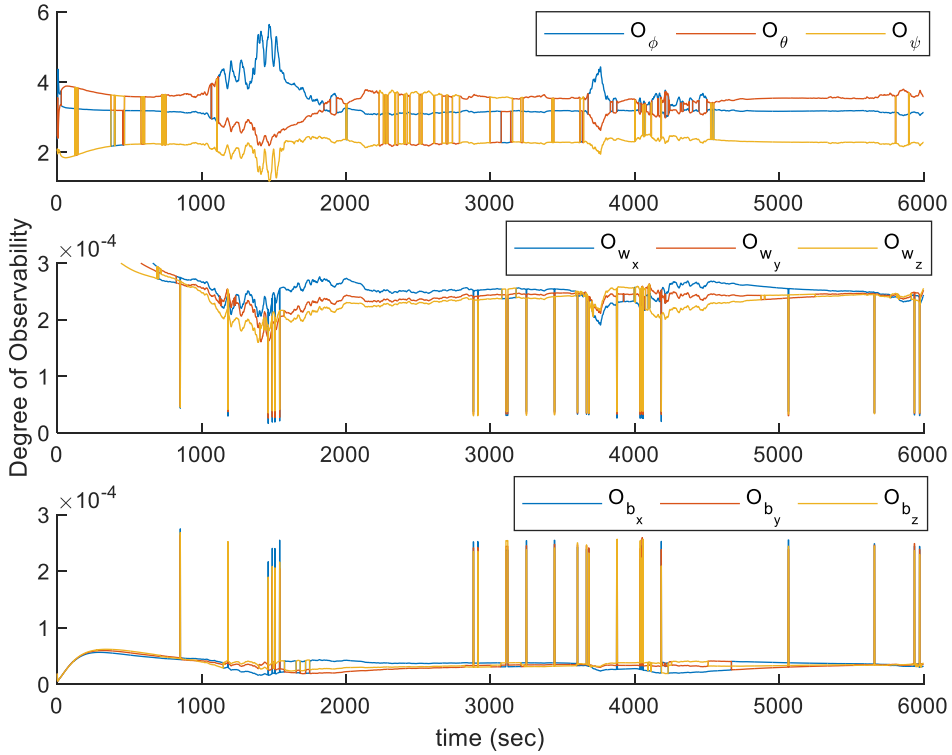

Fig. 13. Degree of observability for each state: Panel 1 for Euler angles, Panel 2 for angular velocities, Panel 3 for gyro biases.

The DoO is presented in Fig. 13. The degrees are presented under the panels as Euler angles in the first, angular velocities in the second, and gyro biases in the third one. The degree is bounded between 0 and 9 with that being smaller means better observability. We see the uphill and downhill changes as a jump since we consider a time span as long as the period of the satellite. However, we can state that the yaw angle is the best observable angle among the other two whereas the angular velocity and bias terms have better observability with very small differences in the components. In Table 1, the RMS errors of the estimations are averaged over 5 simulations for 5 different intervals under 3 scenarios. The first scenario (A) is having a noise increment on the measurements. The next scenario (B) is to have two vector observations becoming parallel. The last case (C) is having a 90º pitch angle that affects both the measurement and system models. In each scenario, it is seen that the SVD-Aided EKF copes better with the erroneous measurement than the traditional EKF. R-Adaptive EKF is slightly better than but very close to SVD-Aided EKF for the first period examined, unlike the other periods. A summary of the filters containing the information of mean, maximum, and standard deviations for the whole period is presented in Table 2. UKF is presented as well in Table 2 for evaluating how much a UKF could improve the EKF results (even they use different ways in approximating the integrals). Given the circumstances of a failure in the measurements, adaptive filters cope well with the faults during these periods. However, it seems that the R-Adaptive filter is more oscillatory than the SVD-Aided EKF.

Table 2. Errors for the attitude estimations (averaged over 5 simulations).

	Mean (deg)	Maximum (deg)	Standard Deviation (deg)
Traditional EKF	0.3586	3.7009	0.5052

UKF	0.2001	2.5083	0.1018
R-Adaptive EKF	0.1004	1.9002	0.2473
SVD-Aided EKF	0.0927	1.8016	0.1194

8. Experimental Verification of SVD-Aided EKF

A test platform is manufactured to allow experimental verification of a satellite's attitude and control algorithms with Euler angle representation. The testbed is used to create and execute test cases that include sensors, actuators, and algorithms. Magnetometers, accelerometers, and gyroscopes make up the sensor suite, which is used to estimate the state. As the principal attitude control actuator, three response wheels are employed on each axis. The primary payload-carrying table, mass balancing blocks, and adapters for equipment installation make up the test setup. To achieve mass balance, coarse balancing blocks are put on the four corners, while fine balancing blocks are positioned on each principal axis. For online analysis, the platform includes a wireless monitoring system and a power distribution unit. In a distributed control mechanism, a computer is employed to manage attitude determination and control duties.

Figure 14 depicts the equipment assembled on the test table. The equipment employed in the primary system is represented by the sensors/IMU, reaction wheels, and modem in the current image. Because the computer is the heaviest piece of equipment, it is positioned in the middle of the test table to match the mass and rotational center. There is also a battery block on the table's bottom surface that goes into the power distribution box. They are symmetrically situated for coarse mass balancing.

Various scenarios for satellite attitude estimation are assessed and studied by applying traditional and nontraditional Kalman-type filters. On the platform, algorithms created for small satellite attitude estimation are evaluated.

The theoretical magnetic field model outputs and magnetometer readings are acquired from the test setup. The test setup magnetometer data and model-based sun sensor vector findings are then employed in the SVD-aided EKF. The suggested attitude estimation technique ensures that satellite attitude estimate converges to real attitude values. The estimation results are shown in Fig. 15 as roll, pitch, and yaw angles along the x, y, and z axes.

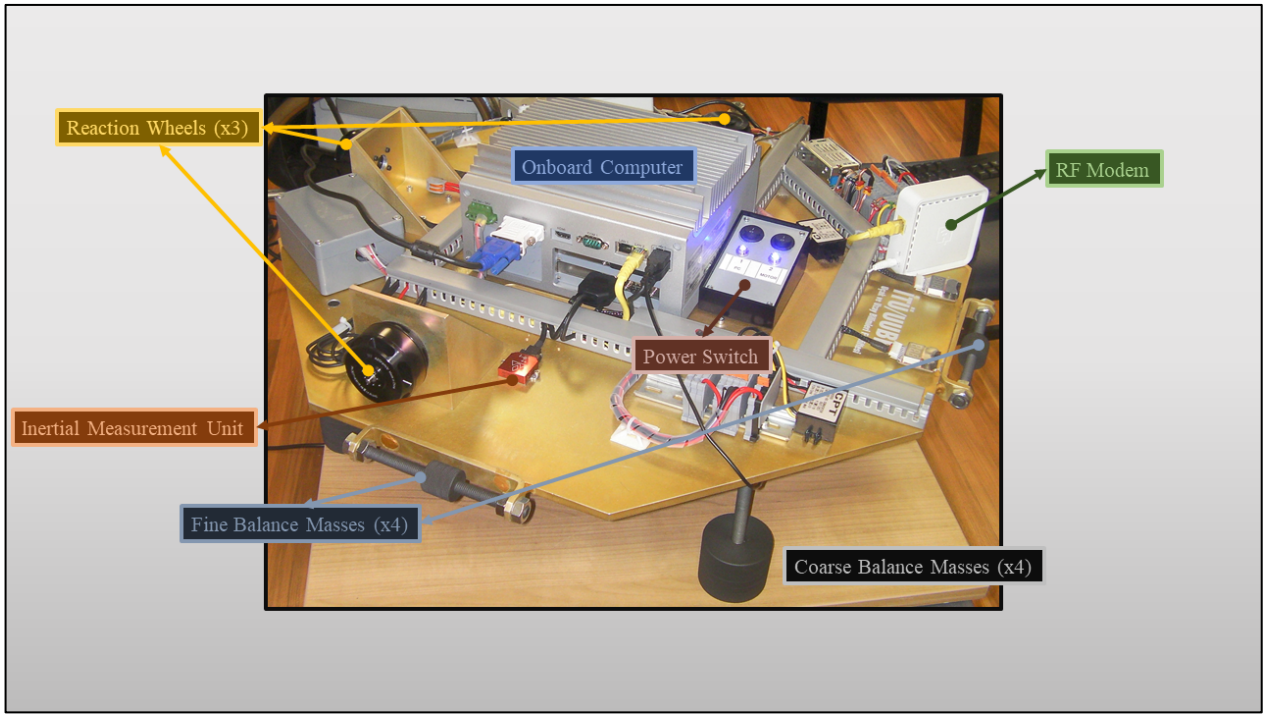

Fig.14. Manufactured test table assembly.

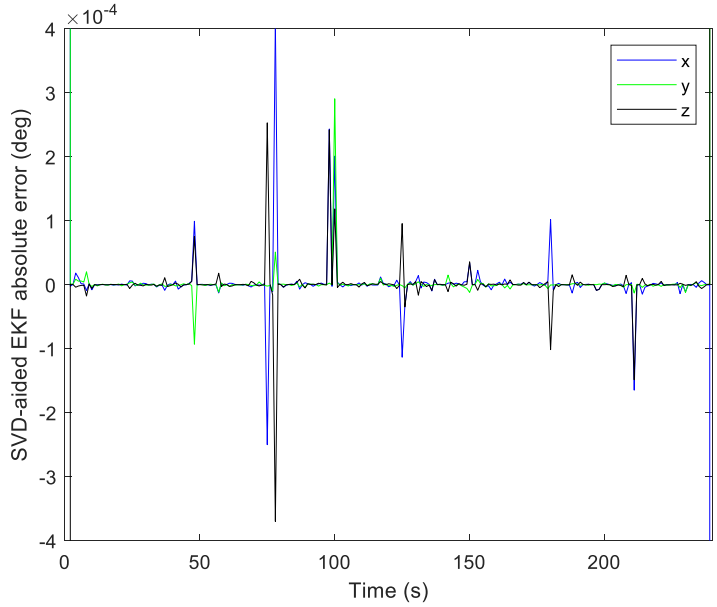

Fig.15. Absolute errors of SVD-aided EKF estimation of the test platform.

9. Conclusion

In this study, the SVD and EKF algorithms are integrated as a two-stage estimation scheme in order to estimate the attitude, angular velocities, and gyro biases of a satellite. In the pre-process, the Wahba's loss function is minimized by SVD using a magnetometer and sun sensors. By using this stage, the attitude measurements and their covariance are used as inputs in addition to rate gyro

measurements for the EKF, which shapes the second stage of the algorithm. SVD's covariance prediction is directly used in the second stage as EKF's measurement noise covariance matrix. The filter is specifically adjusted this way during the eclipse period. It was shown that the EKF improved during the attitude determination stage.

The presented filter has linear measurements, which makes the structure of the filter less complex. Furthermore, the filter is inherently adaptive because the measurement variances are updated every step. The analyses indicated that attitude angles, angular rates, and gyro biases can be accurately estimated with the filter presented. The filter is tested under noise increment fault case, parallel vector observations case, and 90^{o} pitch angle case. From the tests, it is found that the filter copes with these errors well in the sense of estimation accuracy of the attitude angles. The presented filter is also more advantageous in reconfigurability based on the measurement inputs and poorly chosen initial attitude state than the traditional filters, since it uses a preprocessing step. A comparison of the proposed filter with UKF, EKF and adaptive version of EKF is realized for presenting the performances of each filter in different situations. On the test platform, algorithms for estimating the attitude of small satellites are experimentally validated.

References

[1] S. Jo, H. Bang, H. Leeghim, A Vector Measurement-based Angular Velocity Estimation Scheme for Maneuvering Spacecraft, J. Astronaut. Sci. 64 (2017) 310–332. doi:10.1007/s40295-016-0109-x.

[2] C. Hajiyev, D. Cilden-Guler, Review on Gyroless Attitude Determination Methods for Small Satellites, Prog. Aerosp. Sci. 90 (2017) 54–66. doi:10.1016/j.paerosci.2017.03.003.

[3] M.L. Psiaki, F. Martel, P.K. Pal, Three-axis attitude determination via Kalman filtering of magnetometer data, J. Guid. Control Dyn. 13 (1990) 506–514. doi:10.2514/3.25364.

[4] P. Sekhavat, Q. Gong, I.M. Ross, NPSAT 1 Parameter Estimation using Unscented Kalman Filter, in: Proc. 2007 Am. Control Conf., New York, USA, 2007: pp. 4445–4451. doi:10.1109/ACC.2007.4283031.

[5] H.E. Soken, C. Hajiyev, Unscented Kalman Filter Based Attitude Estimation of ITU-PSAT I Satellite Using Magnetometer Measurements, in: Proc. Int. Work. Small Satell. New Mission. New Technol., Istanbul, TURKEY, 2008: pp. 72–76.

[6] T. Inamori, N. Sako, S. Nakasuka, Attitude control system for the nano-astrometry satellite "Nano-JASMINE," Aircr. Eng. Aerosp. Technol. 83 (2011) 221–228. doi:10.1108/00022661111138639.

[7] C. Olson, R.P. Russell, S. Bhaskaran, Spin State Estimation of Tumbling Small Bodies, J. Astronaut. Sci. 63 (2016) 124–157. doi:10.1007/s40295-015-0080-y.

[8] S. Mansoor, U.I. Bhatti, A.I. Bhatti, S.M.D. Ali, Improved attitude determination by compensation of gyroscopic drift by use of accelerometers and magnetometers, Measurement. 131 (2019) 582–589. doi:10.1016/J.MEASUREMENT.2018.08.067.

[9] S. Zhang, G. Chang, C. Chen, L. Zhang, T. Zhu, Attitude determination using gyros and vector measurements aided with adaptive kinematics modeling, Measurement. 157 (2020) 107679. doi:10.1016/J.MEASUREMENT.2020.107679.

[10] H. Rong, Y. Zhu, J. Lv, Y. Chen, C. Peng, L. Zou, Conditional equivalence between Extended Kalman filter and complementary filter for two-vector gyro-aided attitude determination, Measurement. 168 (2021) 108428. doi:10.1016/J.MEASUREMENT.2020.108428.

[11] C. Hajiyev, M. Bahar, Attitude Determination and Control System Design of the ITU-UUBF LEO1 Satellite, Acta Astronaut. 52 (2003) 493–499. doi:10.1016/S0094-5765(02)00192-3.

[12] C. Hajiyev, M. Bahar, Increase of accuracy of the small satellite attitude determination using redundancy techniques, Acta Astronaut. 50 (2002) 673–679. doi:10.1016/s0094-5765(01)00222-3.

[13] J.R. Wertz, Spacecraft Attitude Determination and Control, D.Reidel Publishing Company, Dordrecht, Holland, 2002.

[14] H.E. Soken, S. ichiro Sakai, Attitude estimation and magnetometer calibration using reconfigurable TRIAD+filtering approach, Aerosp. Sci. Technol. 99 (2020) 105754. doi:10.1016/j.ast.2020.105754.

[15] C. Hajiyev, Adaptive filtration algorithm with the filter gain correction applied to integrated INS/Radar altimeter, Part G J. Aerosp. Eng. 221 (2007) 847–885. doi:10.1243/09544100JAERO173.

[16] H.E. Soken, C. Hajiyev, Pico Satellite Attitude Estimation via Robust Unscented Kalman Filter in the Presence of Measurement Faults, ISA Trans. J. Autom. Meas. 49 (2010) 249–256.

[17] C.H. Kang, S.Y. Kim, C.G. Park, A GNSS Interference Identification and Tracking based on Adaptive Fading Kalman Filter, IFAC Proc. Vol. 47 (2014) 3250–3255. doi:10.3182/20140824-6-ZA-1003.01374.

[18] C. Sun, Y. Zhang, G. Wang, W. Gao, A New Variational Bayesian Adaptive Extended Kalman Filter for Cooperative Navigation, Sensors. 18 (2018) 2538. doi:10.3390/s18082538.

[19] B. Zheng, P. Fu, B. Li, X. Yuan, A Robust Adaptive Unscented Kalman Filter for Nonlinear Estimation with Uncertain Noise Covariance, Sensors. 18 (2018) 808. doi:10.3390/s18030808.

[20] H.E. Soken, C. Hajiyev, REKF and RUKF for Pico Satellite Attitude Estimation in the Presence of Measurement Faults, J. Syst. Eng. Electron. 25 (2014) 288–297. doi:10.1109/JSEE.2014.00033.

[21] T. Zhang, X. Xu, Z. Wang, Spacecraft attitude estimation based on matrix Kalman filter and recursive cubature Kalman filter, Proc. Inst. Mech. Eng. Part G J. Aerosp. Eng. 232 (2018) 3024–3033. doi:10.1177/0954410017723359.

[22] C. Hajiyev, D. Cilden, Y. Somov, Gyro-free attitude and rate estimation for a small satellite using SVD and EKF, Aerosp. Sci. Technol. 55 (2016) 324–331. doi:http://dx.doi.org/10.1016/j.ast.2016.06.004.

[23] D. Cilden, H.E. Soken, C. Hajiyev, Nanosatellite attitude estimation from vector measurements using SVD-AIDED UKF algorithm, Metrol. Meas. Syst. 24 (2017) 113–125.

doi:10.1515/mms-2017-0011.

[24] C. Hajiyev, D. Cilden, Y. Somov, Integrated SVD/EKF for small satellite attitude determination and rate gyro bias estimation, in: IFAC Proc. Vol., 2015: pp. 233–238. doi:10.1016/j.ifacol.2015.08.089.

[25] J. Liu, X. Li, Y. Zhang, A. Du, X. Zeng, Y. Yang, A Gyro-Aided Strapdown Triaxial Magnetometer Calibration Method Robust to Gyro Bias, IEEE Trans. Instrum. Meas. 70 (2021). doi:10.1109/TIM.2021.3060594.

[26] W. Wang, T. Lee, Spacecraft Attitude and Gyro-Bias Estimation with a Single Magnetometer on SO(3) ×R3, in: AIAA Sci. Technol. Forum Expo., American Institute of Aeronautics and Astronautics Inc, AIAA, 2022. doi:10.2514/6.2022-0616.

[27] J. Lee, B. Lee, S. Sung, Attitude Estimation Method of High-Spinning Body through Onboard Sensor Fusion under Uniaxial Gyroscope Saturation Environment, IEEE Trans. Instrum. Meas. 70 (2021). doi:10.1109/TIM.2021.3099555.

[28] W. Ding, Y. Gao, Attitude Estimation Using Low-Cost MARG Sensors with Disturbances Reduction, IEEE Trans. Instrum. Meas. 70 (2021). doi:10.1109/TIM.2021.3104395.

[29] B. Candan, H.E. Soken, Robust Attitude Estimation Using IMU-Only Measurements, IEEE Trans. Instrum. Meas. 70 (2021) 1–9. doi:10.1109/TIM.2021.3104042.

[30] E.J. Kim, Y.H. Kim, J.H. Lee, S.J. Park, J.W. Song, S.Y. Park, Gyroscope Bias Estimation Method using Iterated State Transition Fusion Algorithm, ASCC 2022 - 2022 13th Asian Control Conf. Proc. (2022) 2237–2240. doi:10.23919/ASCC56756.2022.9828294.

[31] F. Zhang, X. Lyu, Y. Wang, H. Gu, Z. Li, Modeling and flight control simulation of a quad rotor tail-sitter VTOL UAV, AIAA Model. Simul. Technol. Conf. 2017. (2017). doi:10.2514/6.2017-1561.

[32] M.A. Bek, T. Amer, Y. Gamiel, On the Spinning Motion of a Disc under the Influence a Gyrostatic Moment, Springer Proc. Math. Stat. 364 (2021) 2–14. doi:10.1007/978-3-030-77314-4_1/FIGURES/8.

[33] A. Caubet, J. Biggs, A motion planning method for spacecraft attitude maneuvers using single polynomials, in: Adv. Astronaut. Sci. Astrodyn., 2016: pp. 1445–1461.

[34] D.A. Vallado, Fundamentals of Astrodynamics and Applications (3rd Ed.), Microcosm Press/Springer, USA, 2007.

[35] E. Thébault, C.C. Finlay, C.D. Beggan, P. Alken, E. Al., International Geomagnetic Reference Field: the 12th generation, Earth, Planets Sp. 67 (2015) 79. doi:10.1186/s40623-015-0228-9.

[36] G. Wahba, Problem 65-1: A Least Squares Estimate of Satellite Attitude, Soc. Ind. Appl. Math. Rev. 7 (1965) 409. http://www.malcolmdshuster.com/FC_Wahba_1965_J_SIAM.pdf.

[37] K. Vinther, K.F. Jensen, J.A. Larsen, R. Wisniewski, Inexpensive Cubesat Attitude Estimation Using Quaternions And Unscented Kalman Filtering, Autom. Control Aerosp. 4 (2011).

[38] F.L. Markley, D. Mortari, Quaternion Attitude Estimation using Vector Observations, J.

Astronaut. Sci. 48 (2000) 359–380. doi:10.1007/BF03546284.

[39] L. Markley, Attitude Determination Using Vector Observations and the Singular Value Decomposition, J. Astronaut. Sci. 38 (1987).

[40] D.A. Vallado, P. Crawford, SGP4 orbit determination, in: AIAA/AAS Astrodyn. Spec. Conf., Code available at: "http://www.centerforspace.com/downloads/," Honolulu, Hawaii, 2008. doi:10.2514/6.2008-6770.

[41] D. Cilden-Guler, C. Hajiyev, SVD-aided EKF attitude estimation with UD factorized measurement noise covariance, Asian J. Control. 21 (2019) 1423–1432. doi:10.1002/asjc.1979.

[42] V.M. Popov, Hyperstability of Control Systems, Springer Berlin Heidelberg, 1973. doi:10.1007/978-3-642-65654-5.

[43] N.P.G. Salau, J.O. Trierweiler, A.R. Secchi, Observability analysis and model formulation for nonlinear state estimation, Appl. Math. Model. 38 (2014) 5407–5420. doi:https://doi.org/10.1016/j.apm.2014.03.053.

[44] F.M. Ham, R. Grover Brown, Observability, Eigenvalues, and Kalman Filtering, IEEE Trans. Aerosp. Electron. Syst. AES-19 (1983) 269–273. doi:10.1109/TAES.1983.309446.

[45] B. Dahmane, B. Lejdel, E. Clementini, F. Harrats, S. Nassar, L.H. Abderrahmane, Controlling the degree of observability in GPS/INS integration land-vehicle navigation based on extended Kalman filter, Bull. Electr. Eng. Informatics. 11 (2022) 702–712. doi:10.11591/EEI.V11I2.3695.

[46] R. Mehra, Approaches to Adaptive Filtering, IEEE Trans. Automat. Contr. 17 (1972) 693–698. doi:10.1109/TAC.1972.1100100.

[47] H.E. Soken, C. Hajiyev, S. Sakai, Robust Kalman Filtering for Small Satellite Attitude Estimation in the Presence of Measurement Faults, Eur. J. Control. 20 (2014) 64–72. doi:10.1016/j.ejcon.2013.12.002.

[48] D. Cilden-Guler, M. Raitoharju, R. Piche, C. Hajiyev, Nanosatellite attitude estimation using Kalman-type filters with non-Gaussian noise, Aerosp. Sci. Technol. 92 (2019) 66–76. doi:10.1016/J.AST.2019.05.055.

[49] C. Yang, W. Shi, W. Chen, Comparison of Unscented and Extended Kalman Filters with Application in Vehicle Navigation, J. Navig. 70 (2017) 411–431. doi:10.1017/S0373463316000655.